TURBOMACHINERY & PUMP SYMPOSIA | HOUSTON, TX
DECEMBER 14-16, 2021
SHORT COURSES: DECEMBER 13, 2021

SHANNON'S MACHINE CAPACITY AND DEGRADATION-ENTROPY GENERATION METHODOLOGIES FOR FAILURE DETECTION: PRACTICAL APPLICATIONS TO MOTOR-PUMP SYSTEMS

Juan S. Rincon
VP of Product
Machine Essence Corp.
Austin, Texas, USA

Michael D. Bryant, PhD PE
CEO
Machine Essence Corp.
Austin, Texas, USA

Jude Osara, PhD PE
Assistant Professor
Universiteit Twente
Enschede, Netherlands

Benito R. Fernández, PhD
CTO
Machine Essence Corp.
Austin, Texas, USA

Juan obtained his master's degree in The University of Texas at Austin. After graduating he helped launch Machine Essence, a company dedicated to the diagnostic and prognosis of assets in the Oil and Gas sector. Juan has successfully participated and co-developed workshops for clients such as Chevron, and he has led the product development and has successfully managed an SBIR program grant. Juan's research interests include artificial intelligence, deep neural networks, dynamic systems modeling, robotics, system diagnostics and prognosis, cybersecurity, Internet of Things, and entrepreneurship.

Jude is an assistant professor and the manager of the SKF university technological center at the University of Twente. He obtained his PhD in Mechanical Engineering at The University of Texas at Austin with a dissertation on "degradation thermodynamics", an approach he applied to batteries, grease degradation, general fatigue, and others. Jude is also a licensed Professional Engineer (PE), having worked in the automotive industry as a thermal/fluids engineer, and as an applied mechanics engineer. Between 2017 and 2020, Jude ran his technology start-up EnHeGi, a platform on which he further developed his PhD research into engineering analysis tools for industrial use. EnHeGi was acquired by Machine Essence in 2020. Currently, Jude researches system degradation, life models, failure mechanisms, and materials, all of which he applies his thermodynamics expertise to.

Mike obtained a BS in Bioengineering from The University of Illinois at Chicago in 1972 and a Masters in Mechanical Engineering in 1980 and a PhD in Engineering Science and Applied Mathematics in 1981 from Northwestern University. In 1988 he joined The University of Texas at Austin as a Professor, where he was awarded the Accenture Endowed Professorship of Manufacturing Systems Engineering. Mike was also the editor in Chief of ASME Journal of Tribology. Mike has written over 100+Articles and 5 Patents. Aside from his research Mike has served as a consultant in several companies with immense expertise in industry: Clevite Seals (1985-1988), 3M (1990-92), Onstadt Law (2004-05), Chevron Oronite (2007-2009), King Cycle (2010-2016). Mike is a licensed Professional Engineer. His interests span tribology, mechatronics, design, manufacturing, engineering mechanics and electronics. In 2018, Mike retired from The University to launch Machine Essence, a new venture that focuses on machine diagnosis with his colleague and long time friend Benito.

Benito began his career in Venezuela, where he studied Chemical Engineering in 1979 and Materials Engineering in 1981 at Universidad Simón Bolívar. In 1981, he moved to the US to carry out graduate research at MIT, where he received his MS in 1985 and PhD in 1988, both in Mechanical Engineering. Benito joined The University of Texas at Austin in 1990, where he specialized in Applied Intelligence – use of mixed technologies to create intelligent devices; Nonlinear Robust-Optimal Control; and Mechatronics. His research focus included genetically-evolving neuro-fuzzy systems, automated modeling, system identification, system diagnostics & prognosis of industrial equipment, self-healing circuits, and cyber-physical systems. He has five issued patents and two pending, as well as numerous IP disclosures. In 2017, Benito retired from teaching to pursue his entrepreneurial endeavors.

Copyright© 2021 by Turbomachinery Laboratory, Texas A&M Engineering Experiment Station

ABSTRACT

Current methodologies on health assessment and diagnostics of systems and components are limited in analysis and accuracy. Methodologies like artificial intelligence or limit checks examine statistical significance rather than the actual degradation occurring in the system's components. The authors have demonstrated two approaches based on information theory and thermodynamics to analyze the degradation dynamics and their significance in faults.

In previous publications, the authors have established the similarity between a machine and Shannon's communication channel and the relation between machine degradation and channel capacity [the amount of information that can be transmitted through a given channel]. The authors call this equivalency "Machine Capacity," and it relates to the machine availability to perform the desired work with enough quality and confidence under time and information constraints. Different degradation mechanisms increase Entropy (which decreases Information Entropy used for channel capacity), in particular "modes" that might be detectable under the right conditions and with appropriate sensors. Experimental results have shown that a quick health screening and assessment can be conducted with limited historical data, and can yield definite fault isolation with enough historical data. Additionally, due to its simple implementation, this methodology can be done online with simple computing units.

Degradation of systems –like motor-pumps, compressors, or fans– induce thermodynamic changes. Those changes, related to degradation mechanisms such as friction, fracture, heat transfer, plastic deformation, among others, generate entropy. The methodology in this work quantifies the entropy generated by degradation in a system, correlates this entropy with the rate of specific degradation mechanisms, and shows how it affects particular variables of interest. These methods resulted in the Degradation-Entropy Generation (DEG) Theorem that successfully assessed battery, grease, material fatigue, and motor degradation. DEG models show an impressive near 100% correlation with measured data. Via deviations from baseline values and profiles obtained from a healthy motor pump, this article shows how DEG elements consistently detect faults in the pump, including shaft imbalance, soft foot, and misalignment.

The experimental approaches have demonstrated that this method can be used for failure analysis and fault detection on a variety (any) systems, including pumps, compressors, dry gas seals, valves, fuel cells, etc. This study compares and combines these two methods to understand how they can be used as tools to assess machine health and availability. The process and control data such as voltages, currents, speeds, pressures, temperatures, and flow rates were acquired in several experiments.

INTRODUCTION

Asset diagnosis and prognosis has always been a necessity in the industry to schedule timely maintenance while avoiding catastrophic failures. Machines ultimately fail and current methodologies and solutions are not yielding the results they promised. Basic algorithms like limit-check often oversimplify the underlying issues and conclude in false-positives or missed faults. More complex solutions such as artificial intelligence use pattern recognition to find faults on huge amounts of (big) data with almost no science to back results. These shortfalls in diagnosis and prognosis cost companies millions of dollars every year in maintenance, repairs and loss of production. The authors have demonstrated two approaches based on information theory and thermodynamics that analyze the degradation dynamics. These methodologies look at the underlying problem of degradation towards failure and what it means in terms of the physical model.

HEALTH ASSESSMENT USING SHANNON'S COMMUNICATION THEORY

When a machine is built, even before it is put to work, its components start to degrade. Failure occurs when physical or chemical changes alter the machine's functioning to the point the machine no longer works–defined as when the machine is no longer capable of performing its intended function satisfactorily. While changes induced by degradation can be delayed, failure is inevitable without proper maintenance. This health assessment methodology determines if degradation has increased significantly or if a fault exists on the asset. This methodology quickly assesses a machine's overall health condition without complex simulations or extensive calculations, nor does it require extensive knowledge from the machine and extensive historic data. Under the hood, this methodology applies channel communications theory to machines to measure degradation. The methodology was first introduced by Bryant and Choi (2012) and further demonstrated in industrial applications by Costuros (2013), Bryant (2014) and Rincon (2020).

Shannon's Theorems

Claude Shannon (1948) presented his theories of information, reviewed in "Communication in the Presence of Noise" (Shannon, 1998). Shannon quantified the amount of information contained in a message sent over a communications channel and encoded into a signal by a transmitter. The communications channel is imperfect: the channel contains physical faults that contaminate the signal with noise. The receiver accepts the noisy signal and attempts to extract the message for the destination, despite the noise. This process is shown as block diagrams in Figure 1. A little noise allows recovery of the message. Excessive noise obscures the signal and hampers recovery of the message. Shannon's channel capacity assesses the ability of a communications channel to extract the message from a noisy signal.

Copyright© 2021 by Turbomachinery Laboratory, Texas A&M Engineering Experiment Station

Although Shannon's formulations used probability theory and "information entropy", the channel capacity formulas only involve useful engineering quantities. The channel capacity is the maximum amount of information per unit time that can be transmitted over a channel and successfully extracted from the received signal, despite an amount of noise with power *N* on the channel. The channel capacity formula involves the ratio *S/N* of the powers of signal *S* to noise *N*, and the frequency bandwidth *W* of the channel.

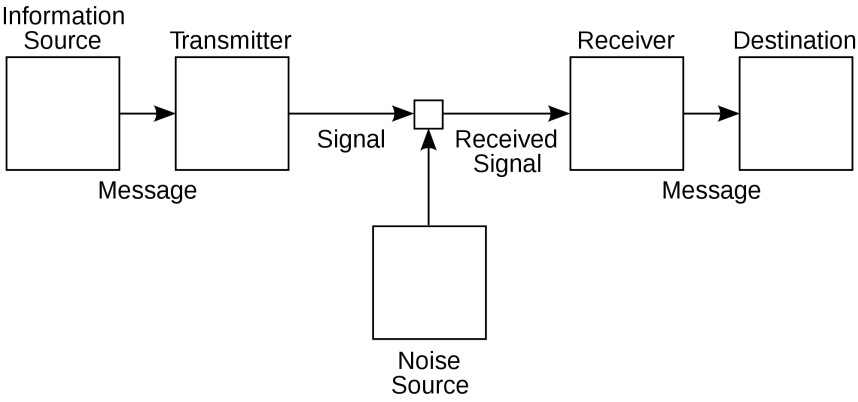

Figure 1. General Communication System (Shannon, 1948)

Theorem: Shannon Channel Capacity (Shannon, 1998)

The capacity of a channel C_{ws} of bandwidth W, involving a received signal of power S_y, contaminated with white Gaussian noise of average power N, is given by

$$C_{ws} = W log_2(\frac{S_y}{N}). \tag{1}$$

If we consider a channel without noise ($N = 0$), the channel capacity of infinity means the transmitted signal can be easily decoded into the original message. Accordingly, if the noise (which obscures the signal) increases, the channel capacity decreases, and less information per unit time can be sent through the channel, received and decoded without error. As S_y/N diminishes, it becomes more difficult to decode the signal into the original message. Implied is that a threshold on S_y/N exists for decoding a signal and extracting the message. This threshold extends to the channel capacity C_{ws}.

White Gaussian noise has a flat or constant amplitude over the entire frequency band of the power spectrum. If non-flat Gaussian noise must be modeled, the channel capacity can be obtained by integrating equation (1) over all frequency bands of the signal and noise power spectral densities, giving

$$C_{ws} = \int_0^w log_2(\frac{S_y(f)}{N(f)})\, df\ , \tag{2}$$

where, the bandwidth W is the highest frequency the channel can conduct. Similar to the white noise model, when the average noise $N(f)$is zero at a given frequency f, the signal-noise ratio $Sy(f)/N(f)$ becomes infinite. Nonetheless, in real world applications noise contaminates all bands of the system, so this state is not observed in practice.

Equations (1) or (2) quantify the physical condition of and ability to send and receive signals over a noisy communications channel. Other theorems of Shannon (1998) quantified the rate *R* of information transmitted by a source, and posed an inequality $R < C$ necessary for the success of a communications channel wherein *R* serves as a threshold of success for the channel capacity *C*. Shannon's theorems are the "Newton's laws" of the multi-trillion dollar communications industry (Internet, television and radio transmissions, data storage and retrieval, among others). If a communications channel obeys the inequality $R < C$, it functions within specifications and it works! Otherwise, it does not work!

Analogy of Machine to Communication Channel

Shannon's theories quantify the ability of a communication channel to perform its function (send and receive information). If the channel degrades, by noise injection, it limits the ability to transmit information effectively. If we compare a machine to a communication channel, we can use Shannon's theory to quantify the ability of a machine to perform its function. A machine transfers power in its various forms (mechanical, electrical, hydraulic, etc.) through the machine's elements to accomplish a task. For example, a pump takes mechanical power (input signal) to generate pressure and flow of a liquid (received signal). Faults in the machine *change the signals* of power flowing through the machine system, equivalent to noise altering the signals that flow through a communication channel. Similar to how noise disrupts the reception of information in a communication channel, faulty components in a machine add 'fault noise' to the power signals flowing through the machine, which prevents the normal functioning of the machine. Signals carrying power through a

Copyright© 2021 by Turbomachinery Laboratory, Texas A&M Engineering Experiment Station

machine can include current, pressure, force, or velocity. A 'Healthy Machine' should produce a desired ideal output signal $y_0(t)$, while a 'Faulty Machine' produces an actual output signal $y(t)$. The machine degradation (fault) in the system perturbs the signal from $y_0(t)$ to $y(t)$. We treat the difference between $y_0(t)$ and $y(t)$ as the induced "fault noise" $n(t) = y(t) - y_0(t)$. With this approach, we can quantify the powers in the signal to noise ratio S_y/N and apply Shannon's channel capacity, equations (1) or (2), to the (machine) channel to assess its ability to perform its function. Changes to the machine's channel capacity, *C,* measures the effects of faults (degradation via fault noise) on the machine's performance.

Health Assessment and Degradation Metric

In an industrial environment, a baseline-signal, $y_0(t)$, measured from a 'healthy' machine indicates an acceptable low-noise machine communication channel. As the machine system degrades, the measured signal will change from the baseline signal. This change represents fault noise, $n(t) = y(t) - y_0(t)$, which reduces the machine's channel capacity *C*. In the end, as faults worsen, channel capacity, *C,* decreases and finally declines below an acceptable limit, the *threshold* for proper machine functioning.

To quantify the system degradation with the channel capacity technique, a baseline is defined, followed by an evaluation of system degradation:

1. Design of Experiments (DOE): Establish a testing procedure where the system has the most variability in its dynamics (Turn on, turn off, loading, Step). The test requires the motor to be excited in as many modes as possible and exercised over its expected operating range. This testing procedure will be used every time data is collected. Variances, such as different sampling rates, different loading conditions, among others, could be interpreted as noise. Especially for systems with nonlinear dynamics.
2. Collect Data on Healthy System: Operate a 'healthy' system at normal conditions and acquire the signals. A small sample, usually five tests, is required to achieve statistical significance.
3. Clean Data on Healthy System: Sync signals so that they have the same starting point and number of samples.
4. Process Data on Healthy System: At each point in time, average all signatures to obtain an average system response. This is the baseline signal y_0.
5. Collect Data on Current Status: Using the same initial testing procedure, operate the system, and acquire the signal. Similar to the baseline, a small sample, usually five tests, is required to achieve statistical significance.
6. Clean Data on Current Status: Sync signals to have the same starting point and number of samples, similar to the baseline measurement.
7. Process Data on Current Status: Extract the noise from each signal by subtracting baseline signal:

$$n_i = y_i - y_{0i} \tag{6}$$

8. Compute Machine Capacity: Calculate the machine (channel) capacity via Equation (1) or (2) where, W is the (executed) sampling frequency that accounts for the bandwidth of the channel.
9. Perform Diagnosis: Calculate the mean machine channel capacity from the signals for diagnostics.
10. Obtain a threshold or critical value of machine capacity. From machines exhibiting unacceptable levels of performance, associate the threshold with that unacceptable machine having the largest machine capacity .

DEGRADATION ENTROPY GENERATION (DEG) METHODOLOGY

Entropy measures disorganization. Manufacturing, which organizes materials into finished components, reduces entropy. Aging and degradation, which disorganizes materials, increases entropy. The thermodynamic degradation entropy generation methods realizing this, relate degradation to the entropy produced by aging and degradation.

Historically, engineering thermodynamics focused on combustion engines, air conditioning and power generation. Beyond these common applications, a typical engineer does not consider thermodynamics as a tool for system analysis. It has been established that entropy, introduced by the Second Law of Thermodynamics to measure a system's microstructural configuration (order or disorder), is a direct function of energy dissipation. With energy dissipation directly correlated with losses and reduced functionality/performance of a machine, entropy generation is fundamental to degradation.

Recently, several works applying thermodynamics to degradation/failure analysis have emerged including work by Kuhn (2016, 2015, 2018), Naderi (2010, 2009, 2011, 2012a, 2012b 2013), among others. While these works show high, albeit limited, consistency and accuracy in characterizing degradation, the authors report significant inadequacies. Some apply only at certain conditions, others apply to specific systems/components. Employing a fundamental denotation of the second law of thermodynamics, the Degradation-Entropy Generation (DEG) methodology directly correlates any system's degradation to its entropy generation, consistently at near 100% accuracy.

The Degradation-Entropy Generation (DEG) theorem (Bryant, et al. 2008), formulated in 2008 after several experimental studies, states

Copyright© 2021 by Turbomachinery Laboratory, Texas A&M Engineering Experiment Station

that a system's transformation of degradation measure w is directly proportional to the entropy generated by the active dissipative processes S_i'. Mathematically,

$$w = \sum_i B_i S_i' \tag{3}$$

where $B_i = \partial w / \partial S_i'$ are degradation coefficients. Details on the DEG theorem, proof and early application can be found in Bryant, et al. (2008). Osara and Bryant (2019a, 2019b 2019c, 2019d, 2020), extending the original DEG theorem and procedure, introduced and demonstrated the new DEG methodology for instantaneous characterization of multi-disciplinary, multi-scale, multi-component systems undergoing nonlinear transformations. Their approach introduced new characteristic geometric elements, in addition to the existing degradation coefficients. Published DEG models characterizing variegated engineering systems include friction induced wear (Bryant, et al. 2008), charge cycling fade of battery capacity and other electrochemical systems (Osara and Bryant 2019a, 2019b, 2020), stress induced general metal fatigue (Osara and Bryant 2019c) and work induced deterioration of grease and other lubricants (Osara and Bryant 2019d).

DEG Procedure

1. Identify the active dissipative mechanisms that are driving the degradation.
2. Formulate phenomenological entropy generation including all active mechanisms.
3. Select an appropriate parameter, the degradation measure *w*, that describes and quantitatively measures the degradation.
4. Measure system properties in the entropy generation formulation along with the chosen degradation measure.
5. Plot entropy generation terms against degradation measure.
6. Evaluate degradation coefficients B_i as the slopes of the planes on which the degradation-entropy generation plot lays.
7. Re-combine the B_i coefficients with entropy generation to evaluate the system's phenomenological transformation that instantaneously combines the effects of active mechanisms. These transformations are used in degradation/failure monitoring.

Osara and Bryant, applying this procedure, derived and named the Degradation-Entropy Generation (DEG) geometric elements Osara and Bryant (2019a, 2019b 2019c, 2019d, 2020, 2021):

- *DEG trajectory*: the multi-dimensional plot of the degradation parameter vs. entropy generation components, with increasing time tracing consecutive points on the trajectory;
- *DEG plane*: the planar surface on which the DEG trajectory lays;
- *DEG domain*: the multidimensional space enclosing the DEG plane.

Figure 2 shows an example of these planes for battery fade (degradation), with degradation parameter *w* being the maximum charge the battery can hold at the current time (the max charge fades over time). The entropy generations pertain to internal Joule work dissipation (ohmic entropy) and equilibration of internal mass/electro-chemical diffusion/mass transport and heat (ECT entropy). To relate the battery maximum charge to the two entropies, the DEG trajectory is plotted in a 3D space of charge versus entropies. Using standard computational algorithms the goodness of fit of the DEG trajectory to the DEG plane was near 100% and partial slopes of this plane with respect to the entropy axes become the B_i coefficients of degradation in Equation (3).

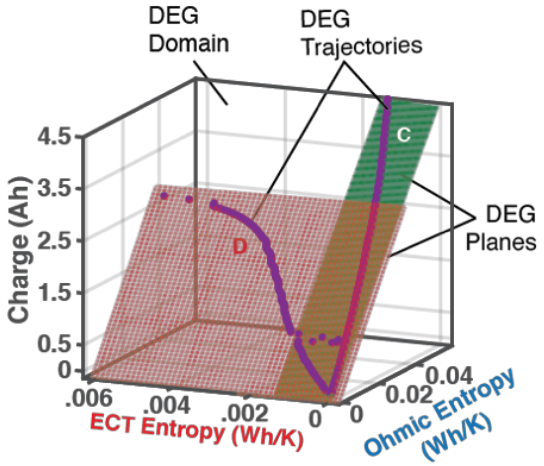

Figure 2. A lithium-ion battery's DEG geometric elements for discharge and charge processes Osara and Bryant (2020).

Thermodynamics of Open Systems

Open systems are systems through which mass and energy flow. Examples are pumps, compressors, pipe networks, valves and others. The first law of thermodynamics, a statement of energy conservation, for a non-reacting system (open and closed) is

Copyright© 2021 by Turbomachinery Laboratory, Texas A&M Engineering Experiment Station

$$\dot{U} = \sum \dot{Q} - \sum \dot{W} + \sum (u + Pv)\, \dot{\mathrm{N}}_e \tag{4}$$

where $\dot{U}$ is the system's internal energy change rate, $\sum \dot{Q}$ sums the rates of heat transfers into and out of the system, $\sum \dot{W}$ sums all external work transfer rates by and on the system, and $\sum (u + Pv)\, \dot{\mathrm{N}}_e$ sums energy flows in and out of the system via mass flow $\dot{\mathrm{N}}_e$ (Osara and Bryant 2021). The second law of thermodynamics for an open system is

$$\dot{S} = \sum \frac{Q}{T} + \sum \frac{(u + Pv)\, \dot{\mathrm{N}}_e}{T} + \dot{S}' \tag{5}$$

where $\dot{S}$ is the rate of entropy change in the system, $\sum \frac{Q}{T}$ sums all entropy transfer rates into and out of the system via heat, $\sum \frac{(u+Pv)\, \dot{\mathrm{N}}_e}{T}$ sums all entropy transfer rates into and out of the system via mass flow, and $\dot{S}'$ is the system's entropy generation rate (Osara and Bryant 2021). Rearranging Equation (5) as $\sum Q + \sum (u + Pv)\, \dot{\mathrm{N}}_e = T\dot{S} - T\dot{S}'$, and substituting the left side into Equation (4) yields the combined form of the first and second laws of thermodynamics for a non-reacting system (open and closed),

$$U = T\dot{S} - \sum \dot{\mathrm{W}} - T\dot{S}' \tag{6}$$

which is rearranged to obtain entropy generation,

$$\dot{S}' = \frac{1}{T}(T\dot{S} - \sum \dot{\mathrm{W}} - \dot{U}) \tag{7}$$

Equation (7), applicable to all systems, open and closed, requires knowledge of entropy and internal energy changes as the system outputs or receives work. Currently, entropy measurement devices do not exist: entropy must be calculated from other measurements. Osara and Bryant (2021) combined Equation (7) with the Helmholtz free energy, a thermodynamic potential that adequately characterizes externally loaded systems, to obtain a more convenient measure of entropy generation

$$\dot{S}' = \frac{\sum [(\dot{m}\, s\, T)_{out} - (\dot{m}\, s\, T)_{in}]}{T} - \sum \frac{\dot{\mathrm{W}}}{T} \tag{8}$$

which monitors instantaneous transformation of a loaded open system using readily measured properties: inlet/exit temperatures T and pressures (used to evaluate inlet/outlet specific entropies s), mass flow rates $\dot{m}$ and power $\dot{\mathrm{W}}$. Examples of loaded open systems are compressors and pumps. Unloaded open systems are pipe networks, valves, etc., for which $\dot{\mathrm{W}}$=0. The first right side term in Equation (8) is the microstructure thermal (MST) entropy S'_{MST} and the second term is the work or load entropy S'_W. For more on the detailed derivation of Equation (8), please see Osara and Bryant (2021).

Open systems such as compressors, pumps, gas seals, etc., often monitor pressure drop across the inlet and outlet as an indication of performance and degradation. The effects of leaks, fouling, motor components degradation and other performance-impacting mechanisms can be observed in the system's pressure drop. As such, using pressure drop ΔP as the transformation measure w in Equation (3), and substituting Equation (8) into Equation (3) yields the DEG governing equation or model for open non-reacting systems,

$$\Delta P = B_{MST} \frac{\sum [(\dot{m}sT)_{out} - (\dot{m}sT)_{in}]}{T} - B_w \sum \frac{\dot{\mathrm{W}}}{T} \tag{9}$$

where B_{MST} is the microstructure thermal (MST) degradation coefficient measuring the impact of the MST entropy on pressure drop, and B_w is the work degradation coefficient measuring the impact of the external work entropy on pressure drop. Both coefficients are obtained from the orthogonal slopes of the DEG plane (recall $B_i = \partial w / \partial S_i'$), as explained previously, and demonstrated subsequently.

Understanding Entropy via the DEG Theorem

Entropy is a measure of disorganization. As such, for the entropy generations of Equations (8) and (9):

- Work or load entropy S'_W: Measures the dissipative and damaging effects of the external (boundary) loads on the system, such as input torques, forces, flows or pressures. This work provides much of the energy that disorganizes a material's microstructure, which degrades the material.
- Microstructure Thermal (MST) entropy S'_{MST}: Measures the dissipative internal response to all prevalent processes such as the

Copyright© 2021 by Turbomachinery Laboratory, Texas A&M Engineering Experiment Station

thermal damage done to materials by the transfer of heat dissipated by the mechanical work.

In most systems, $S'_W \gg S'_{MST}$. The DEG coefficients B_w and B_{MST}, via the DEG theorem, are influence functions that predict the contribution of the entropy terms to system degradation (recall $B_i = \partial w / \partial S_i'$). In systems degrading at a slow rate, the external interaction (often a load or energy input) contributes most significantly to the system's degradation. Examples are closed systems in which $B_w S'_W \gg B_{MST} S'_{MST}$ (the load or the external work interaction dominates the degradation). In open systems, $B_{MST} S'_{MST}$ has an external component (via flow rate $\dot{m}$) with contribution comparable to that of S'_W, i.e., $B_w S'_W \sim B_{MST} S'_{MST}$ These phenomena can be seen in the spatial orientation of the DEG plane within the DEG domain. Contrast the orientations of the DEG planes in Figure 2--for a battery (closed system)--and Figure 12--for a pump (open system).

MOTOR-PUMP SYSTEM DESCRIPTION

Experiment

To test the effectiveness of these two methodologies, experiments were designed on an industrial centrifugal pump, see Figure 3(a). A Motor-Pump system in a circulation loop is very common in industry, where a fluid taken from a source (typically a reservoir) is pumped through a circuit as part of a process. Typical examples are Cooling Water recirculation systems, and, at higher scales, boiler water pumping systems. The selection of the arrangement for this particular application was the high likelihood of similar systems in industrial applications. The pump is powered by a three-phase 15-HP motor. The motor runs at 1760 RPM and has a maximum constant current of 19 Amps with the 480 volts configuration. The motor in its non-driver end has 6206 deep groove ball bearing and in its driver end 6309 deep groove ball bearing. The motor is attached to the pump with a four-way flexible coupling that permits minor misalignment and limits vibration transmission in the system. The pump circulates water at 260-GPM through a network pipe that ends in a tank. Monitored parameters shown in Table 1, include voltage, current, 3-axial acceleration on all bearings, shaft speed, shaft displacement, static pressure at the inlet, static pressure at the outlet, dynamic pressure at the inlet, dynamic pressure at the outlet, flow rates, and motor and pump temperatures. While data from several sensors were recorded, each methodology used a small set of recorded data. Data was sampled at about 16 kHz to get a bandwidth of about 8 kHz and different fault modes were simulated. The faults of interest were:

- Baseline "Healthy", i.e., no imposed faults
- Phase Unbalance
- Shaft Imbalance
- Misalignment
- Soft Foot

Figure 3(a). Motor Pump used for the experiment

Table 1. List of sensors used in the experiments

Sensor	**Range**	**Accuracy**
Voltage Probes	0 $kV$to ± 15 kV	$\pm 1\%$
Current Probes	0.1 Apk to 2000 Apk	$\leq 1\%$
Static Pressure PT Outlet	1.5 psi to 5000 psi	0.1%

Copyright© 2021 by Turbomachinery Laboratory, Texas A&M Engineering Experiment Station

Static Pressure PT Inlet	$\sim 0\ psi$ to $300\ psi$	$\pm 1.5\%$
Dynamic Pressure PT	$\sim 0\ psi$ to $200\ psi$	$2\ mpsi$
Flow Meter	$0.01\ m/s$ to $25\ m/s$	$\pm 0.5\%$
Tachometer	$30000\ RPM$	0.1%
Accelerometers	$\pm 200\ g\ pk$	$0.0002\ g\ rms$
Displacement Probes	$10\ mills$ to $90\ mils$	$\pm 1\%$
Thermocouples	$-40\ °C$ to $70\ °C$	$<\ 0.07\ °C$

Phase Unbalance of a three-phase motor occurs when one or more phases are mismatched. Three-phase power systems and equipment are designed to operate with all three phases balanced. Usually, a motor can safely operate the variance of a few volts, as long as it does not exceed 1% of the maximum voltage. The unbalanced voltages cause unbalanced currents in the motor windings, which increases the current amplitude and winding temperature. Over time these winding temperatures tend to deteriorate the insulation and create a turn-to-turn short. We simulated this fault by adding 200 ft. of 12 AWG[1] to one of the phases. The excess wire would create an added small voltage drop due to about 0.3169 Ω resistance and a small inductance added the affected phase. The wire was tied in a circular manner to counter the induction effects produced by the current flowing through this cable (Geiger, 1982) (Isermann and Freyermuth, 1991) (Thomsen and Kallesoe, 2006).

Shaft Imbalance is produced when the center of gravity of the rotating equipment does not coincide with its center of rotation. This disparity creates unwanted centrifugal forces, which produce excessive vibration in the shafts. This fault could lead to bearing failure, distorted seals and shaft bending. We induced this fault by affixing an eccentric 50g weight to the shaft, Figure 3(b). Note that the imbalance is attached on the pump side.

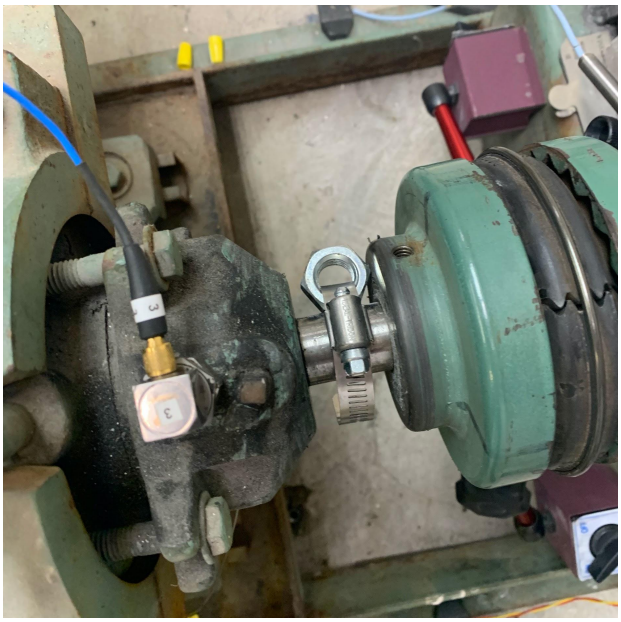

Figure 3(b). Mechanical Unbalance experiment.

The next induced fault was shaft Misalignment. There are two types of misalignment, parallel and angular. Misalignment causes unwanted forces and stress on the shaft of the pump and the motor, which could lead to early shaft fatigue and bearing failure. We induced this fault by adding $0.1\ in$ shims to the back of the motor, causing a $9.5\ mils/in$ angular misalignment and $52.6\ mils$ parallel offset.

[1] 12 American Wire Gauge, solid wire with resistance of about 1.5844 mΩ/ft.

Copyright© 2021 by Turbomachinery Laboratory, Texas A&M Engineering Experiment Station

The last induced fault, soft foot, occurs when a motor is not properly secured to a stable base or plate due to bent or damaged supports, bolts incorrectly torqued, or corrosion of the base or foot. Over time this fault can cause bearing failure, seal deterioration, bent shaft, and excessive vibration. We induced this fault by softening (loosening) one of the bolts at the non-driver end (NDE).

Standard Accelerometer Diagnosis

Current technologies such as vibration analysis and frequency spectral analysis are challenging to implement, and scale poorly. They usually require an expert to analyze data and/or complex, unreliable artificial intelligence algorithms to detect anomalies. As a diagnosis baseline, we performed a vibration analysis on data to compare our solution to good vibration practices as presented on (SKF Reliability Systems 2000). Power spectral density results in Figures 4-11 have baseline data marked with blue points, and fault data marked with orange points.

Table 2. Motor Bearing Fundamental Frequencies

	Driver End 6309 Bearing	**Non-Driver End 6206 Bearing**
Ball Pass Frequency Inner Race (BPFI)	148 Hz	162 Hz
Ball Pass Frequency Outer Race (BPFO)	91 Hz	107 Hz
Fundamental Train Frequency (FTF)	11 Hz	12 Hz
Ball Pass Frequency	60 Hz	70 Hz

The Phase Unbalance did not present any significant change in the spectrum or the amplitude of the acceleration. This is consistent with electrical faults which have to be very severe in order to diagnose with vibration analysis. Shaft imbalance produced very little fault indication and misalignment and soft foot suggested a possible fault. In any of the tests a bearing fault was not detected concluding that the induced faults had not affected the bearing in the motor or pump. A further analysis in the envelope detection concluded that the system did not have any detectable bearing fault because the magnitude was not significant and did not align with fundamental bearing frequencies.

In the shaft imbalance fault, the vibration analysis resulted in very little increment as seen in Figures 4 and 5. For this type of fault, the vibration should indicate a significant increase in the first harmonic in all radial vibration, in this case horizontal vibration and vertical vibration. However the data only indicated a 10% - 15% increase. The shaft imbalance is not seen on the motor accelerometers because the flexible coupling is damping most of the vibration. However, similar behavior is shown on the pump accelerometers where axial vibration increased little.

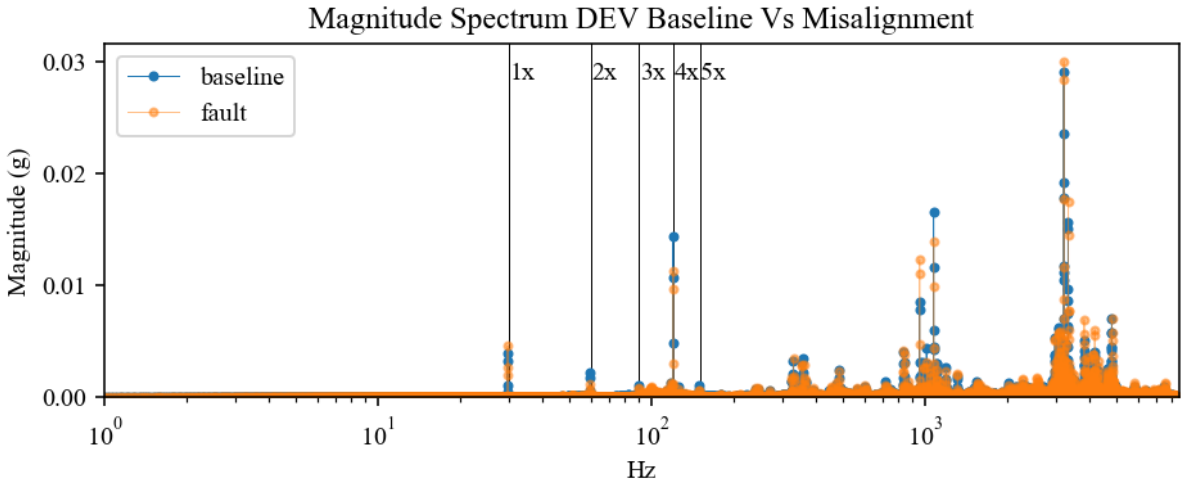

Figure 4. Experimental results: Driver-End Vertical vibration spectrum for Shaft Imbalance.

Copyright© 2021 by Turbomachinery Laboratory, Texas A&M Engineering Experiment Station

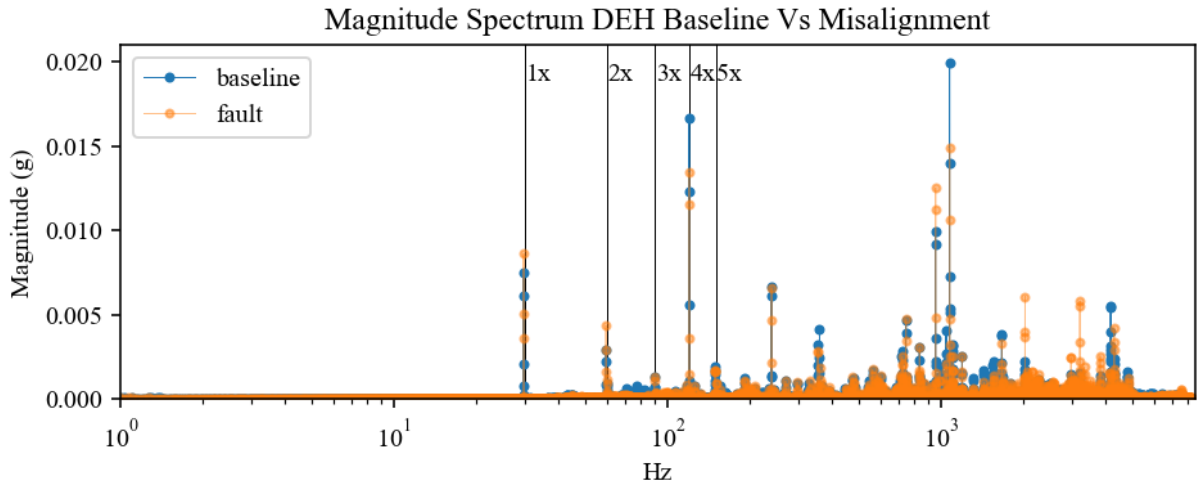

Figure 5. Experimental results: Driver-End Horizontal vibration spectrum for Shaft Imbalance.

For angular misalignment the dominant frequency [~30 Hz] should cause the axial vibration to increase 100% - 200%. In our analysis, that increase was only 10%. For parallel misalignment the dominant frequency is 2x on radial vibrations. While on the vertical vibration in Figure 7 the magnitude of 2x did not increase, on the horizontal vibration in Figure 8 significantly increased. This behavior suggests that the parallel misalignment might be more severe than the angular. The analysis did not yield severe misalignment, but it might be a result of the flexible coupling.

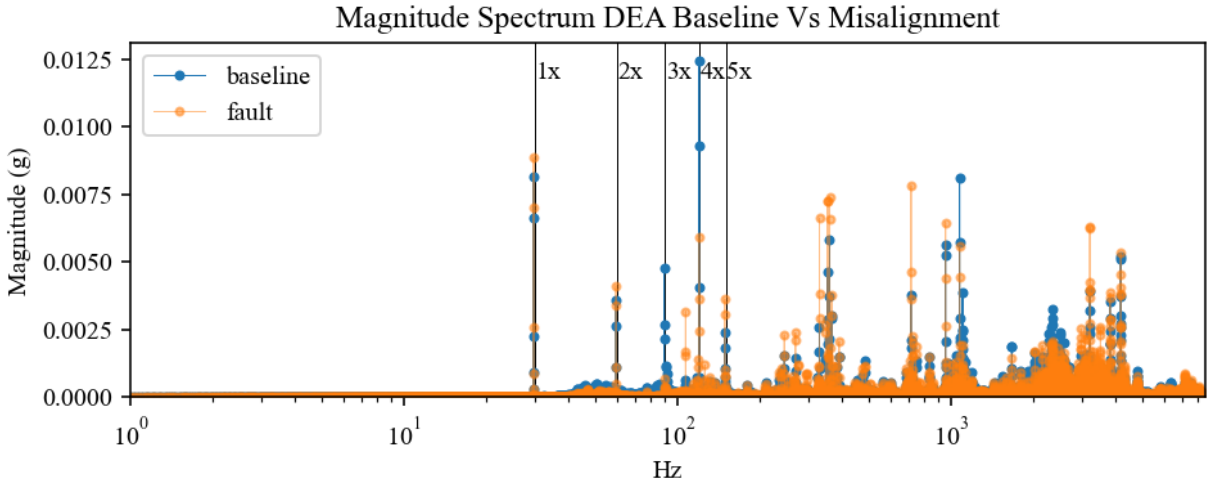

Figure 6. Experimental results: Driver-End Axial vibration spectrum for Misalignment.

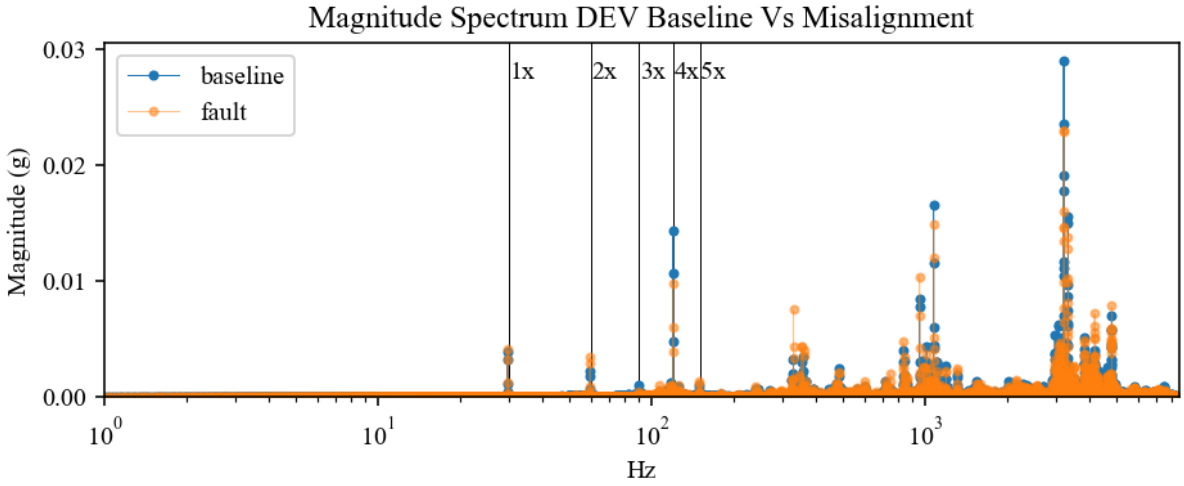

Figure 7. Experimental results: Driver-End Vertical vibration spectrum for Misalignment.

Copyright© 2021 by Turbomachinery Laboratory, Texas A&M Engineering Experiment Station

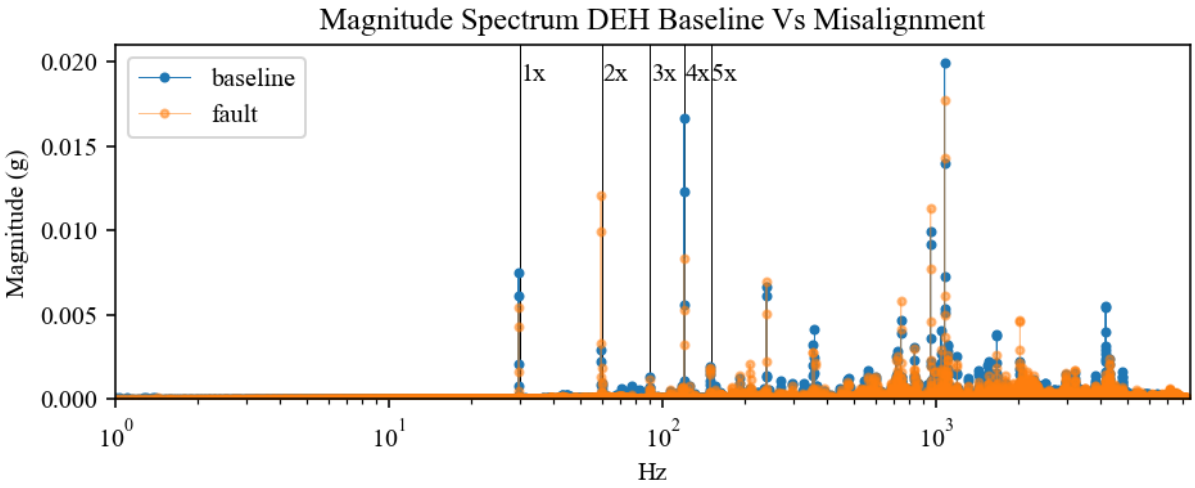

Figure 8. Experimental results: Driver-End Horizontal vibration spectrum for Misalignment.

The Soft Foot vibration analysis yielded better results. Axial and vertical vibration on the non-driver end increased significantly almost 100%, and the axial vibration on the driver end increased to almost 200%. Additionally, several harmonics increased between 20% -30% suggesting a soft foot.

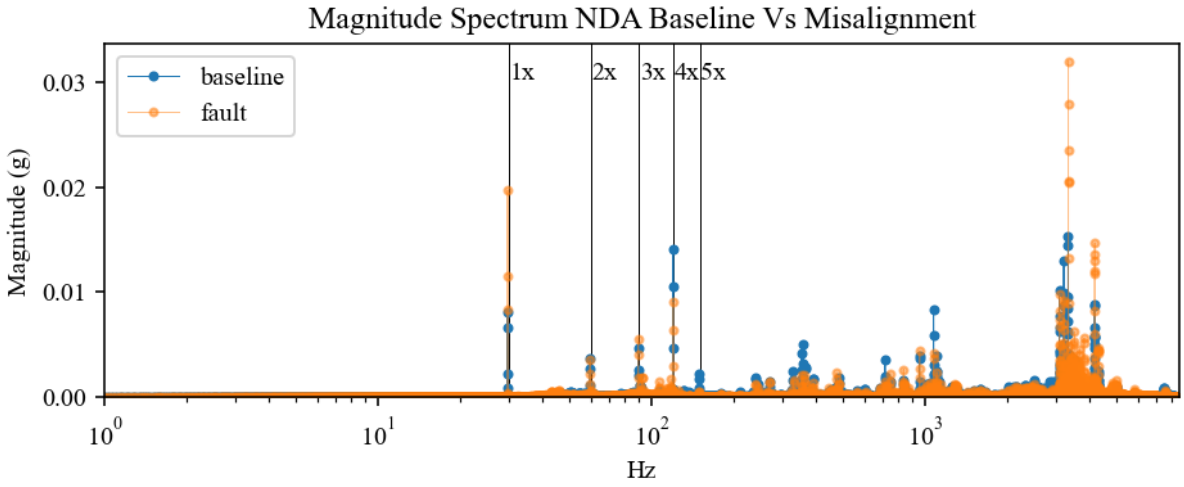

Figure 9. Experimental results: Non-Driver-end Axial vibration spectrum for Soft Foot.

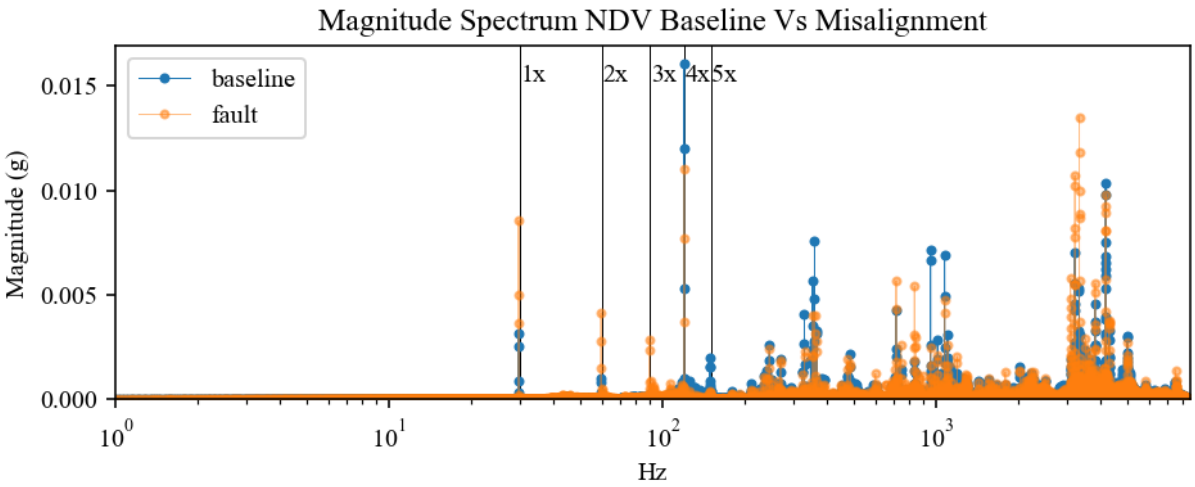

Figure 10. Experimental results: Non-Driver End Vertical vibration spectrum for Soft Foot.

Copyright© 2021 by Turbomachinery Laboratory, Texas A&M Engineering Experiment Station

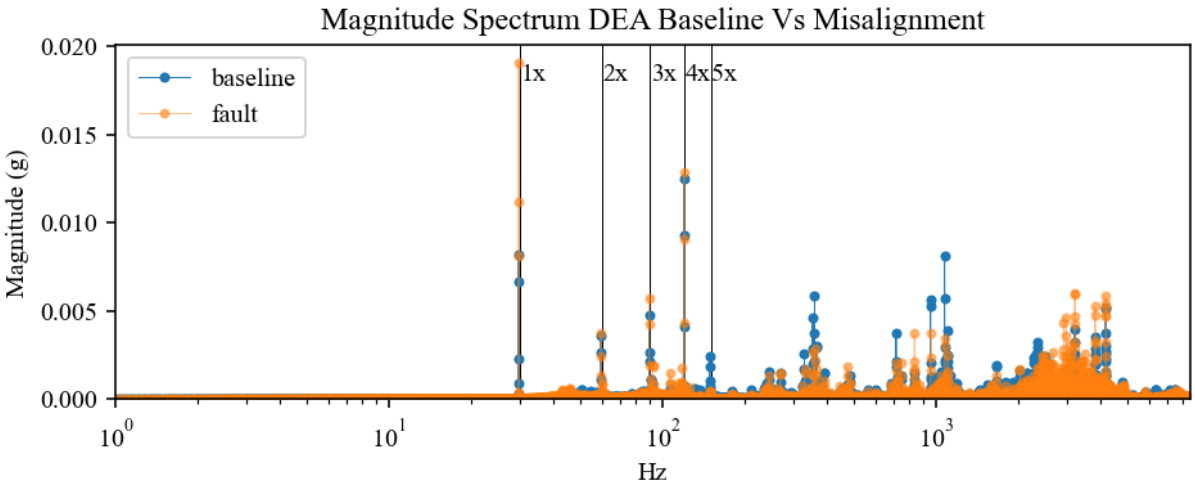

Figure 11. Experimental results: Driver End Axial vibration spectrum for Soft Foot.

APPLICATION OF FAILURE DETECTION METHODOLOGIES TO MOTOR-PUMP DATA

Shannon's Machine Capacity

Instantaneous power [P(t) = V(t) i(t)], was chosen as the signal for this methodology because many faults can be observed by the current/motor torque. Also, by using the input as a reference we can subtract any input noise coming from the voltage lines. Tables 3-7 for various numbered tests (column 1) present machine channel capacity values (column 2) and the ratio of each test value to the baseline Test 1 value (column 3), for each machine condition: baseline, motor stator phase unbalance, shaft imbalance, shaft misalignment and soft foot. Figure 12, which plots these same channel capacity values and averages for each test group (red line), shows significant separation between average values for Baseline healthy and faulty systems.

Table 3. Experimental results: Baseline Machine Channel Capacity (MCC).

	Baseline Results	
	Channel Capacity	**Ratio to Baseline (Test 1)**
Test 1	61,349	1.00
Test 2	68,274	1.11
Test 3	55,791	0.90

Table 4. Experimental MCC results: Phase Unbalance.

	Phase Unbalance Results	
	Channel Capacity	**Ratio to Baseline (Test 1)**
Test 4	33,901	0.55
Test 5	33,889	0.55
Test 6	33,618	0.54

Table 5. Experimental MCC results: Shaft imbalance.

	Shaft Imbalance Results	
	Channel Capacity	**Ratio to Baseline (Test 1)**
Test 7	51, 718	0.84
Test 8	53, 420.	0.83
Test 9	53, 420.	0.87

Table 6. Experimental MCC results: Misalignment.

	Misalignment Results	
	Channel Capacity	**Ratio to Baseline (Test 1)**
Test 10	54, 693	0.89
Test 11	52, 926	0.86
Test 12	52, 768	0.86

Copyright© 2021 by Turbomachinery Laboratory, Texas A&M Engineering Experiment Station

Table 7. Experimental MCC results: Soft Foot.

	Soft Foot Results	
	Channel Capacity	**Ratio to Baseline (Test 1)**
Test 13	53,515.22	0.87
Test 14	52,578.38	0.85
Test 15	50,939.55	0.82

Since all faults showed a distinct drop in their average channel capacity value from the average value of the Baseline healthy system, it was possible to discriminate a healthy system from a faulty system using the "red lines". Additionally, the algorithm was robust against occasional sensor failure. This became evident during test 3 of the baseline, when the sensor presented occasional failure on the voltage reading, which sometimes would shoot to 8000V, which was unrealistic for the 480 volt system. After detecting this sensor fault, the probe was adjusted and this error was not seen in subsequent tests. Nonetheless, the channel capacity was able to overcome occasional sensor failure. The health assessment yielded similar results, whether at start up, steady state or during a loading operation.

The Phase Unbalance fault indicated a channel capacity decrease of 45% (calculated from the red line averages), suggesting a considerable decline in system functional performance. This was expected to have considerable impact on the channel capacity since the fault directly affected the motor current signal used as "sensor" for the assessment. On the other hand, Shaft Imbalance, Misalignment and Soft Foot faults only decreased the capacity of the machine about 15%. These faults resulted in similar size motor current channel capacities because all physically manifested as vibrations that deformed the air gap between the stator and rotor, which changed the air gap magnetics of the motor, which in turn produced slight changes in the motor currents that the algorithm recognized. Hence, although the motor current "sensor" has different (lower) sensitivities to the vibration manifestation of these faults, with this methodology we were able to categorize between two different classes of faults: an electrical Phase Unbalance fault caused by altered motor electrical gear versus mechanical faults of Shaft Imbalance, Misalignment and Soft Foot rendered by air gap disturbances.

By thresholding, the channel capacity can be a health screening technique. Threshold calibration would compare channel capacity values to human assessments of the same system performance, similar to Costuros (2013) and Bryant (2014). In column 3 Tables 3-7, a threshold on the Ratio to Baseline of 0.9 would detect all faults, given sensors operating within reasonable limits.

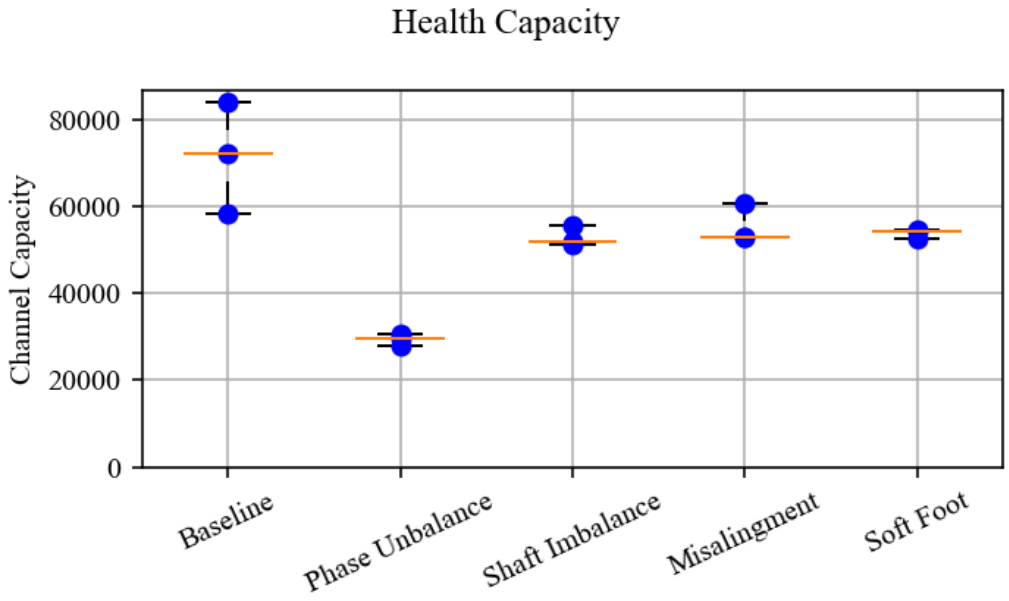

Figure 12. Experimental results: Machine Channel Capacity for all experiments group by Failure Mode. The red lines are averages over the test values of a given fault group.

Degradation-Entropy Generation

All experiments included an initial 7-minute unloaded region followed by a two-step increase in back pressure (loading the pump). Figure 13 shows some of the parameters used in the DEG analysis: inlet and outlet pressures, pressure drop, and flow rate of the fluid. Measured inlet and outlet temperatures of the fluid for each experiment were

- healthy pump: 18.836°C to 18.84°C
- soft foot, misalignment, shaft imbalance and phase unbalance: 16.302°C to 16.308°C.

Copyright© 2021 by Turbomachinery Laboratory, Texas A&M Engineering Experiment Station

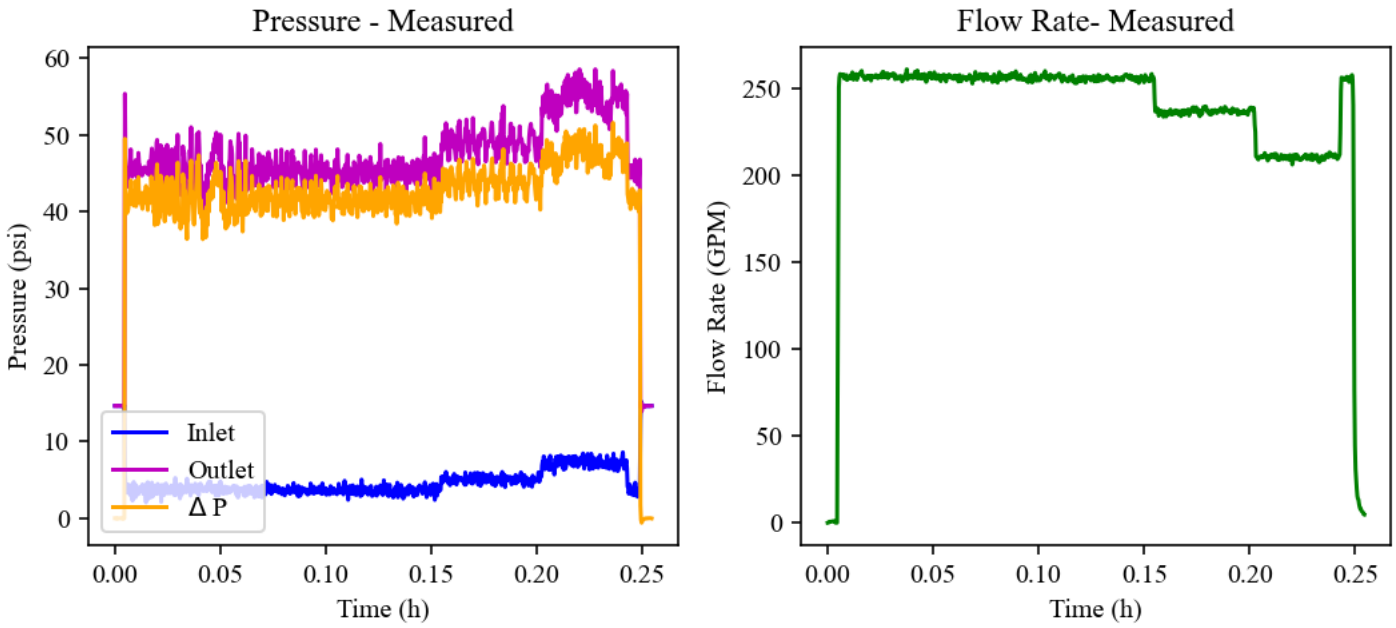

Figure 13. Available experiments measured variables: inlet and outlet pressures, flow rate and temperatures (not shown, ~18.83-18.84°C) during healthy pump operation. Note the operating condition changed and there is some (relatively small) noise in the measurements.

Using instantaneous temperatures and pressures at the inlet and outlet of the pump, specific entropy of water was evaluated during the pump's operation. Following the DEG procedure stated in the previous section, we substituted the measured pressure drop, power, flow rates, temperatures and evaluated entropies into the DEG model. Then, we plotted the pressure drop against the (various) components of entropy generation $S_{SMT}$and S_W (in this case), and obtained a curve fit of the data to a plane, in order to obtain the coefficients of the DEG elements. Results from measured data show the DEG-predicted linear transformation as a function of entropies, per Equation (13), renders a consistent behavior in all datasets processed. Figure 14 shows the DEG elements obtained for a healthy pump, with $B_{MST} = 46.28$ and $B_w = 0.8878$. The degradation coefficients for all tests are shown in Table 8.

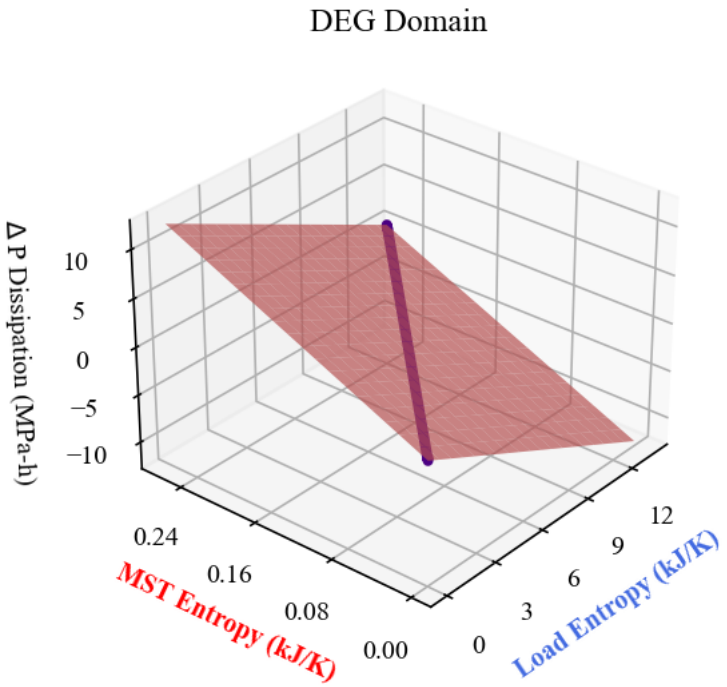

Figure 14. DEG elements obtained from a healthy pump, used in DEG model calibration.

Copyright© 2021 by Turbomachinery Laboratory, Texas A&M Engineering Experiment Station

Table 8. Experimental results: Degradation Entropy Generation Analysis

Condition	B_W	B_{MST}	Comments (Relative to Healthy State)
Healthy/No Fault	0.8878	46.28	--
Phase Unbalance	0.825	42.89	Both B_W and B_{MST} drop slightly to indicate slight degradation with slight fluctuations. (Low to Average Observability).
Shaft Imbalance	0.5896	38.54	B_W drops significantly and B_{MST} drops significantly to indicate consistent degradation. (High Observability).
Misalignment	0.6463	42.23	B_W drops significantly and B_{MST} drops slightly to indicate consistent degradation. (High Observability).
Soft Foot	0.6182	46.68	B_W drops significantly and B_{MST} drops slightly to indicate consistent degradation. (High Observability).

Prognosis: Phenomenology and Dissipation Monitoring

Recombining the degradation coefficients B_w and B_{MST} with the entropy generation components S'_W and S'_{MST} yields phenomenological pressure drop (Phen ΔP) which includes the simultaneous effects of flow rates, temperatures and pressures hitherto unobservable in the measured pressure drop. In the plots on the left side of figures 15, Phen ΔP (Baseline) is the DEG model-predicted phenomenological pressure drop/rise evaluated by combining the current dataset's B coefficients with the current dataset's entropies. Phen ΔP (Actual) is the phenomenological pressure drop/rise evaluated by combining the calibration dataset's B coefficients with the current dataset's entropies.

In the right plots, Baseline Dissipation is the difference between cumulative Measured ΔP and cumulative Phen ΔP (Baseline). Actual Dissipation is the difference between cumulative Measured ΔP and Phen ΔP (Actual). Dissipation Del = Actual-Baseline is the difference between Baseline and Actual Dissipations. Measured datasets are grouped into two categories:

1. Calibration/Baseline data: measured during healthy system operation. Calibration degradation B coefficients for Equation (13) were calculated from these datasets (see above).
2. Faults data: measured during faulty system operation. Calibration degradation B coefficients estimated in item 1 were combined with the faults data to determine actual phenomenological pressure drop, Phen ΔP (Actual). Faults degradation coefficients were combined with the faults data used to determine baseline pressure drop, Phen ΔP (Baseline).

Data from five conditions (one healthy, four faulty) were processed: *Healthy/Baseline, Soft Foot, Misalignment, Shaft Imbalance* and *Phase Unbalance*. Figure 15 presents condition observability signals (phenomenology and dissipation plots). Other detailed DEG analysis plots are in appendix A. Various subfigures of Figure 15 give data for the cases:

- **Healthy** (Figure 15 a) shows DEG-predicted phenomenological pressure drops (Phen ΔP Baseline and Phen ΔP Actual), and measured pressure drop (Measured ΔP) are very close during healthy operation, left plot. The curves often overlay.
- **Soft foot, misalignment and shaft imbalance faults** (Figure 15 b, c, d) show significant negative separation from the baseline—left side plots titled "Phenomenology (PRESSURE DROP)"—which increases dissipation rate (slope of "Del" in the right side plot titled "Dissipation - MONITORING").
- **Soft foot, misalignment and shaft imbalance faults** (Figure 15 b, c, d) appear to show the same amount of dissipation. This similarity is also evident in the flow rates associated with all three faults.
- **Phase unbalance fault** (Figure 15 e) shows low but observable positive separation from baseline. This indicates low dissipation rate, which is verified by the similar flow rates of both phase unbalance and healthy conditions (see detailed DEG analysis plots in appendix A). However, the direction of the separation is also an anomaly indicator.

Note that measured pressure drop ΔP, which is used as a transformation (or degradation) measure, is similar for ALL conditions. Whereas DEG's phenomenological pressure drops, combining the effects of flow rates, pressures and temperatures instantaneously, show the actual changes in the system's behavior, which is not observed in measured pressure drop. For this study, inlet and exit temperatures are assumed atmospheric. See detailed DEG analysis in Figure 16 of appendix A.

Copyright© 2021 by Turbomachinery Laboratory, Texas A&M Engineering Experiment Station

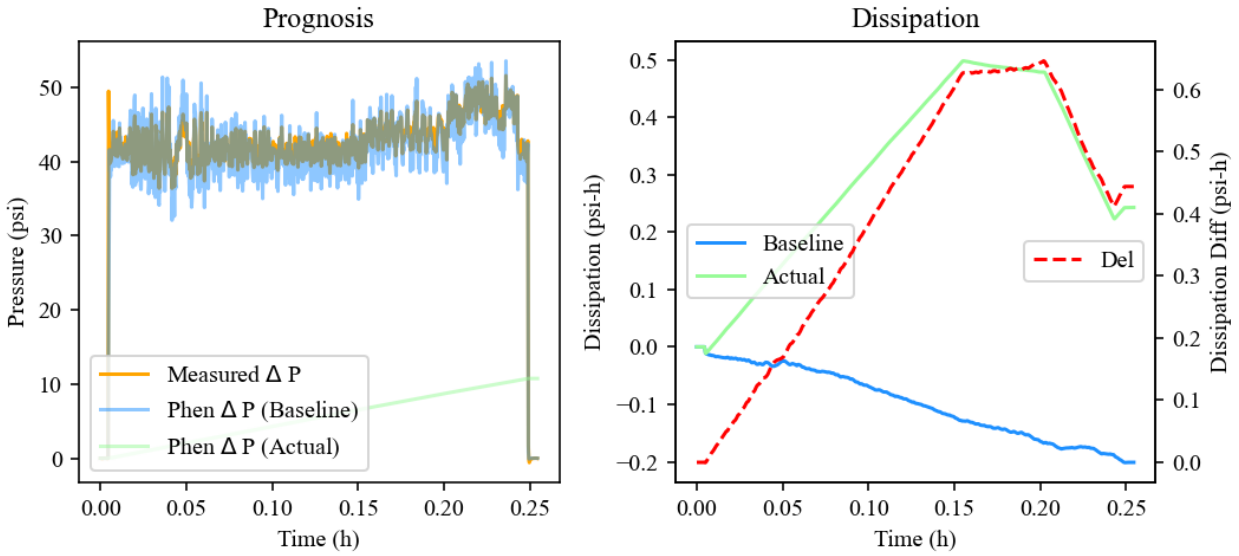

(a) Healthy pump

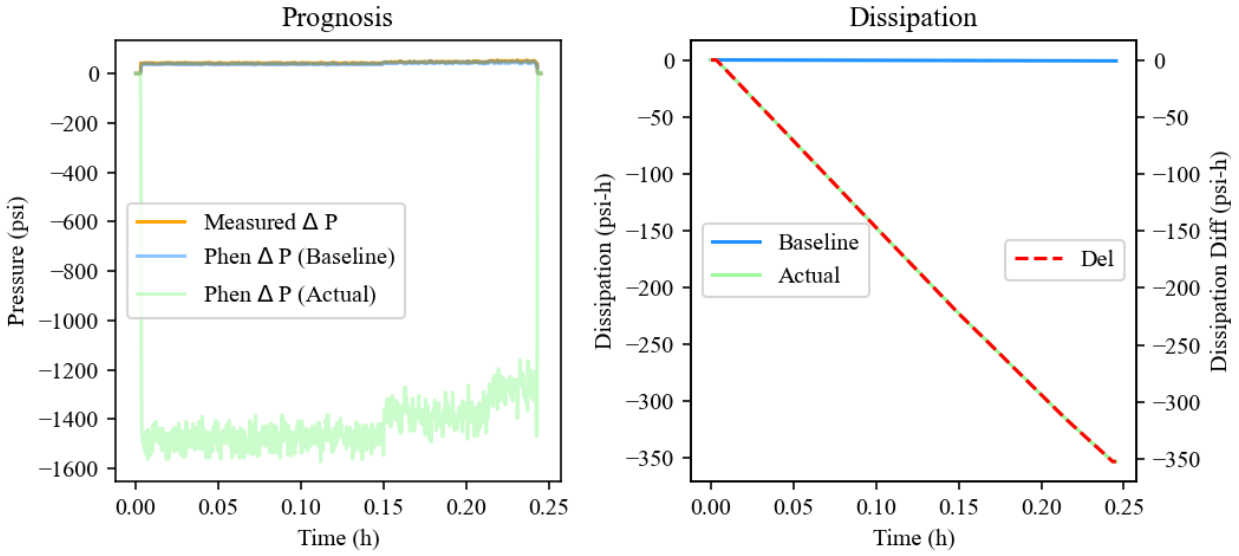

(b) Pump with a soft foot fault condition.

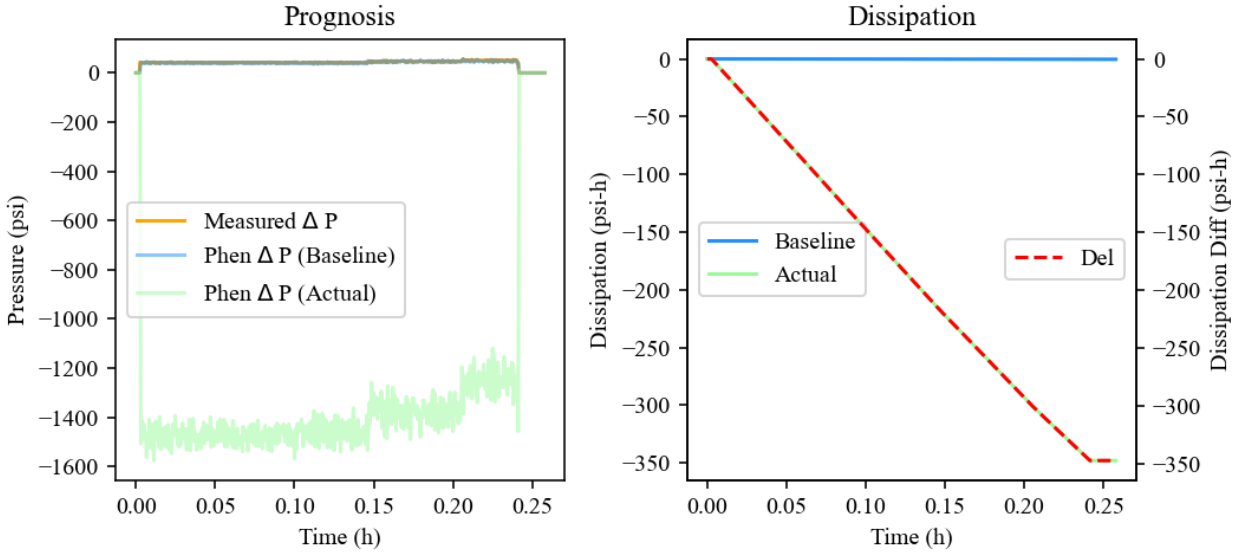

Copyright© 2021 by Turbomachinery Laboratory, Texas A&M Engineering Experiment Station

(c) Pump with a misalignment fault condition.

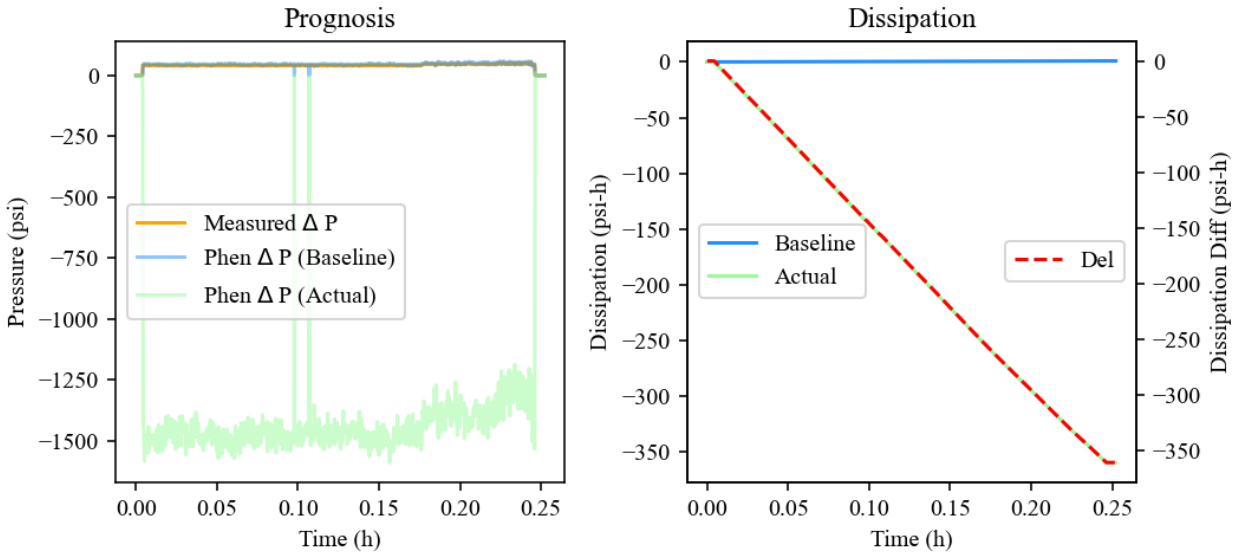

(d) Pump with shaft imbalance fault condition

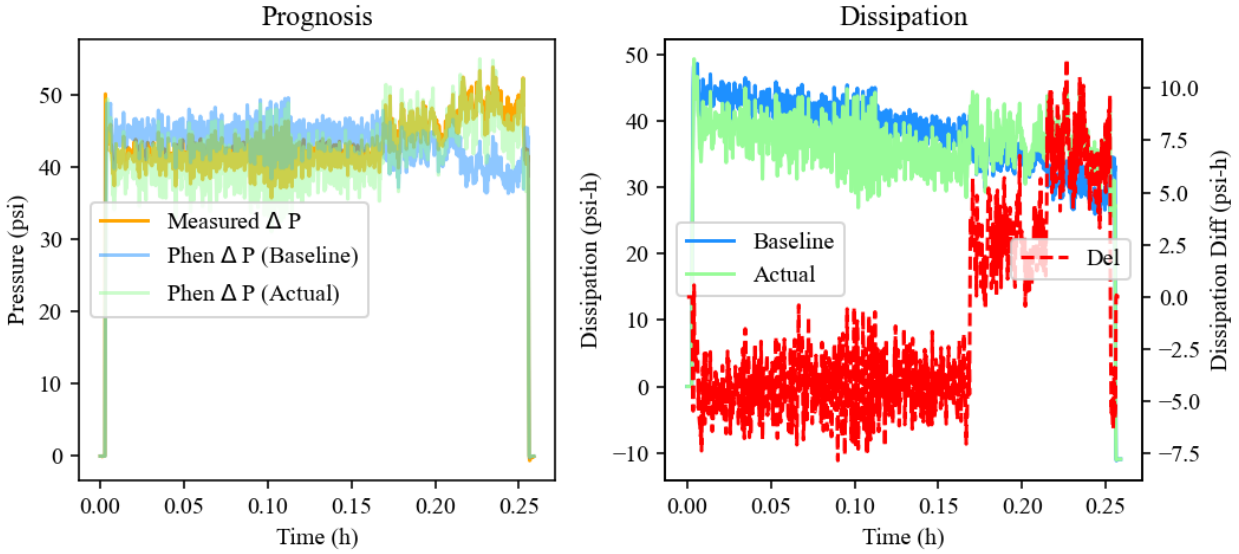

(e) Pump with phase unbalance fault condition

Figure 15. Phenomenology and dissipation monitoring of the motorized pump during healthy and faulty operations. Phen ΔP is phenomenological pressure drop.

Data from additional tests, similar to Figures 13-15, are given in Appendix A.

CONCLUSIONS

This article detailed the practical applications of two novel technologies to degradation/health analysis and fault monitoring of an industrial motor pump system. A machine channel capacity signal monitoring approach, based on Shannon's information theory, was reviewed and applied to fault conditions typically observed in pump operation. The Degradation-Entropy Generation (DEG) methodology based on the DEG theorem was reviewed, a new entropy generation formulation for open systems presented, and the new DEG model applied to the experimental data from the motor pump. Motor-pump faults investigated and observed include soft foot, misalignment, shaft imbalance and phase unbalance. Both methodologies presented in this article show significant capabilities in observing/detecting degradation/failure of the motor pump (or other machinery) and its accessories, as long as the degradation mechanism impacts any of the typically observable system states (temperatures, pressures, flow rates, motor voltages and currents, shaft

Copyright© 2021 by Turbomachinery Laboratory, Texas A&M Engineering Experiment Station

vibrations and shaft speed). The techniques presented did not account for discrimination between the different faults, which was outside the paper's objective and scope. Results showed the different faults to be observable (detectable) with the sensors used, but the proposed techniques using vibration measurements were not able to detect the electrical phase unbalance. Similarly, for the misalignment fault, the vibration analysis results were marginal: the Machine Capacity was able to detect the misalignment fault, but was the less sensitive of all the faults, but with enough statistical significance. For fault classification, additional metrics from different sensors may render the faults distinguishable. This will be our next effort.

APPENDIX A

Presented in Figure 16 are the typical components of a DEG Analysis: monitored parameters during pump operation (inlet and exit pressures, volumetric flow rate and ambient temperature), and DEG elements (entropies, DEG domain, phenomenology and dissipation), for all the investigated conditions.

a) Healthy:

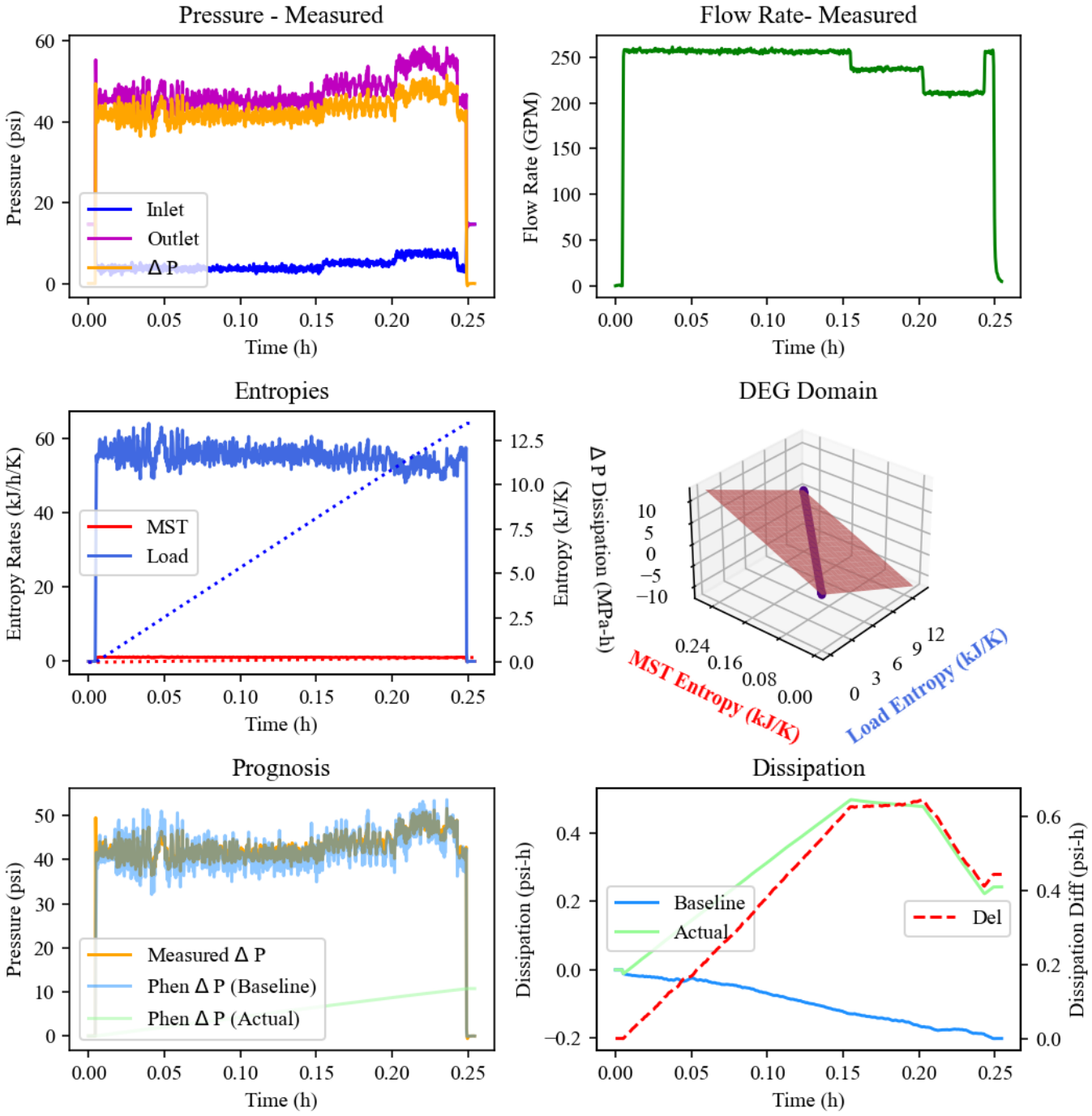

Copyright© 2021 by Turbomachinery Laboratory, Texas A&M Engineering Experiment Station

b) Soft Foot:

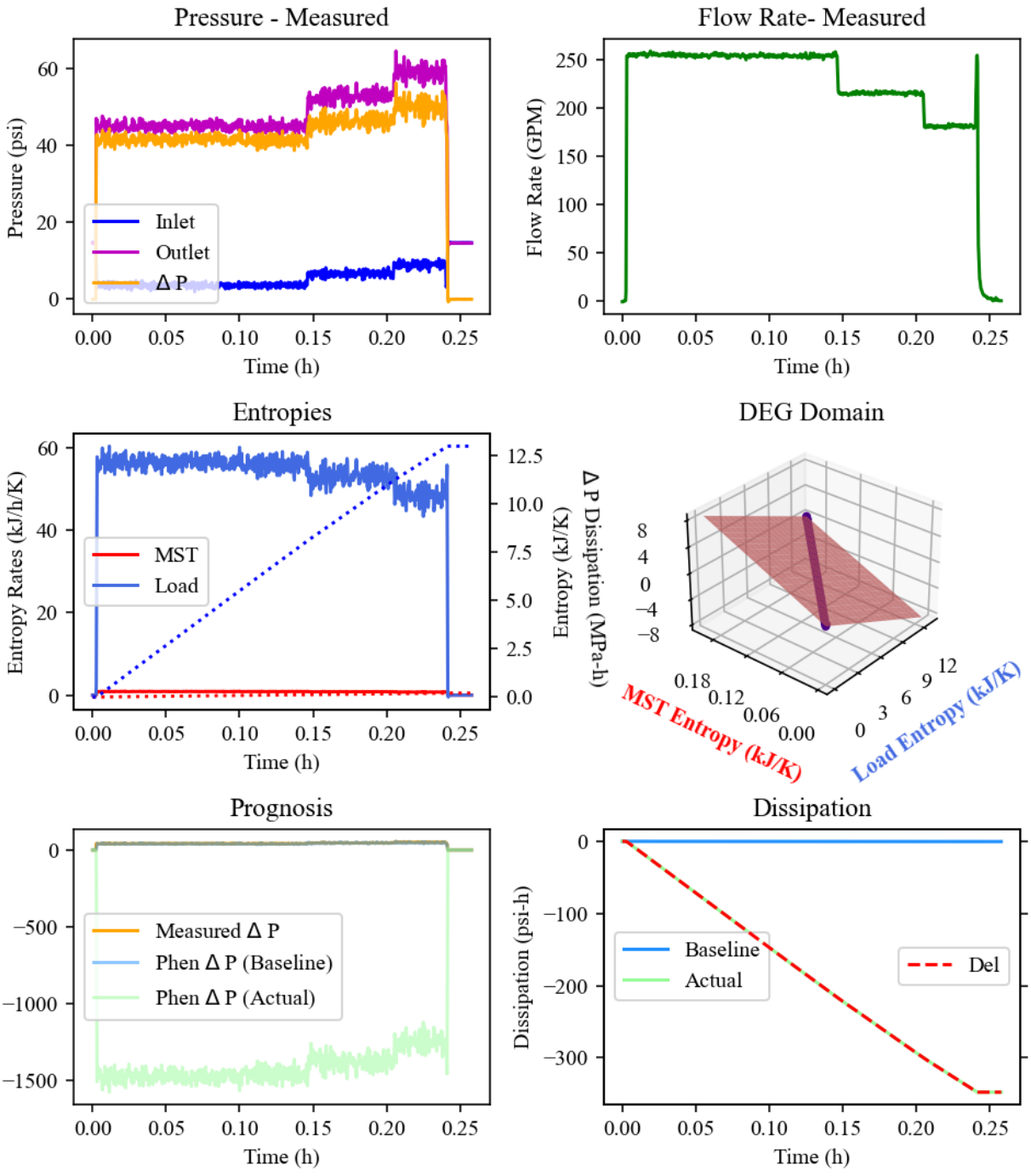

Copyright© 2021 by Turbomachinery Laboratory, Texas A&M Engineering Experiment Station

c) Misalignment:

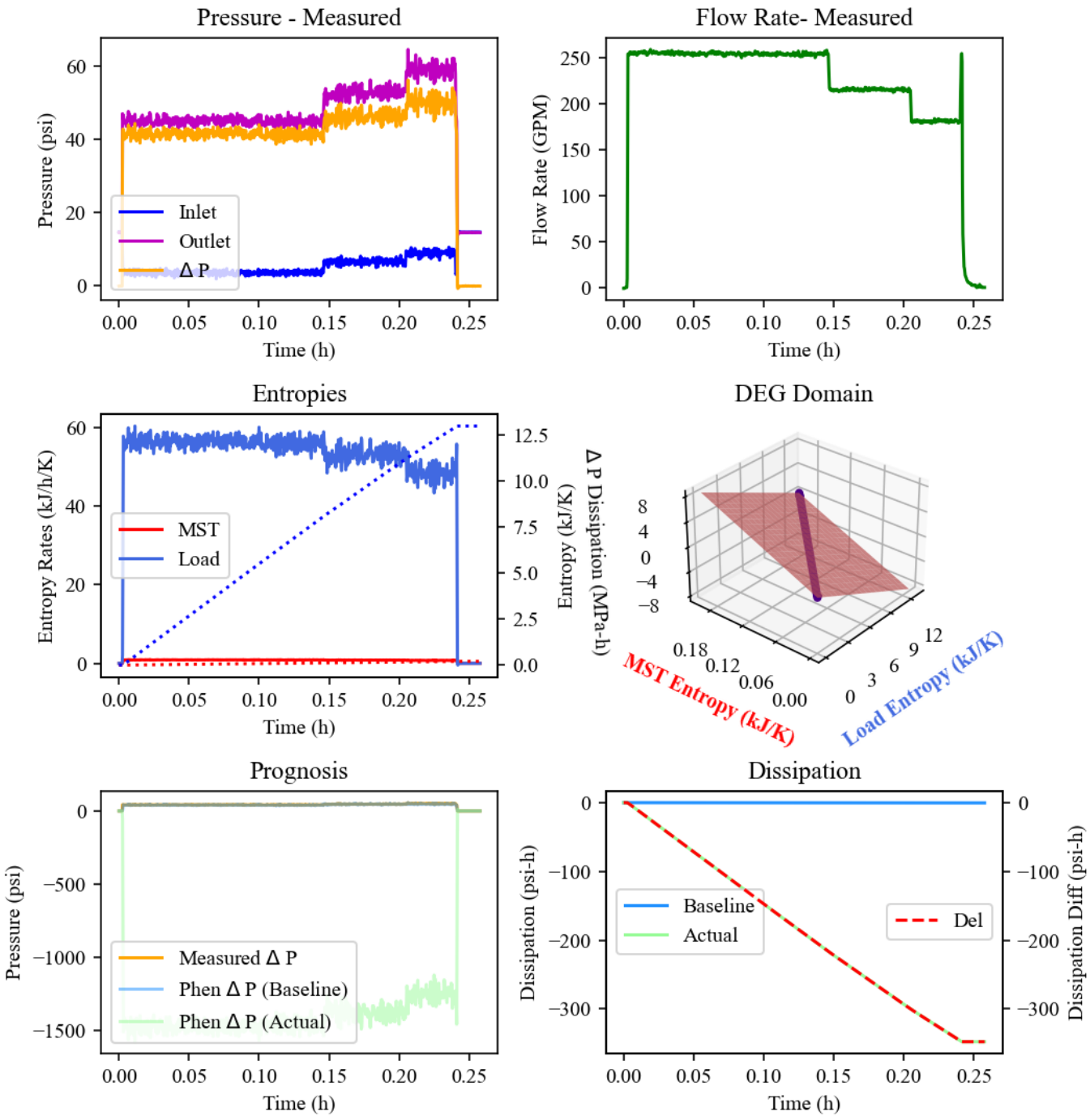

Copyright© 2021 by Turbomachinery Laboratory, Texas A&M Engineering Experiment Station

d) Shaft Imbalance:

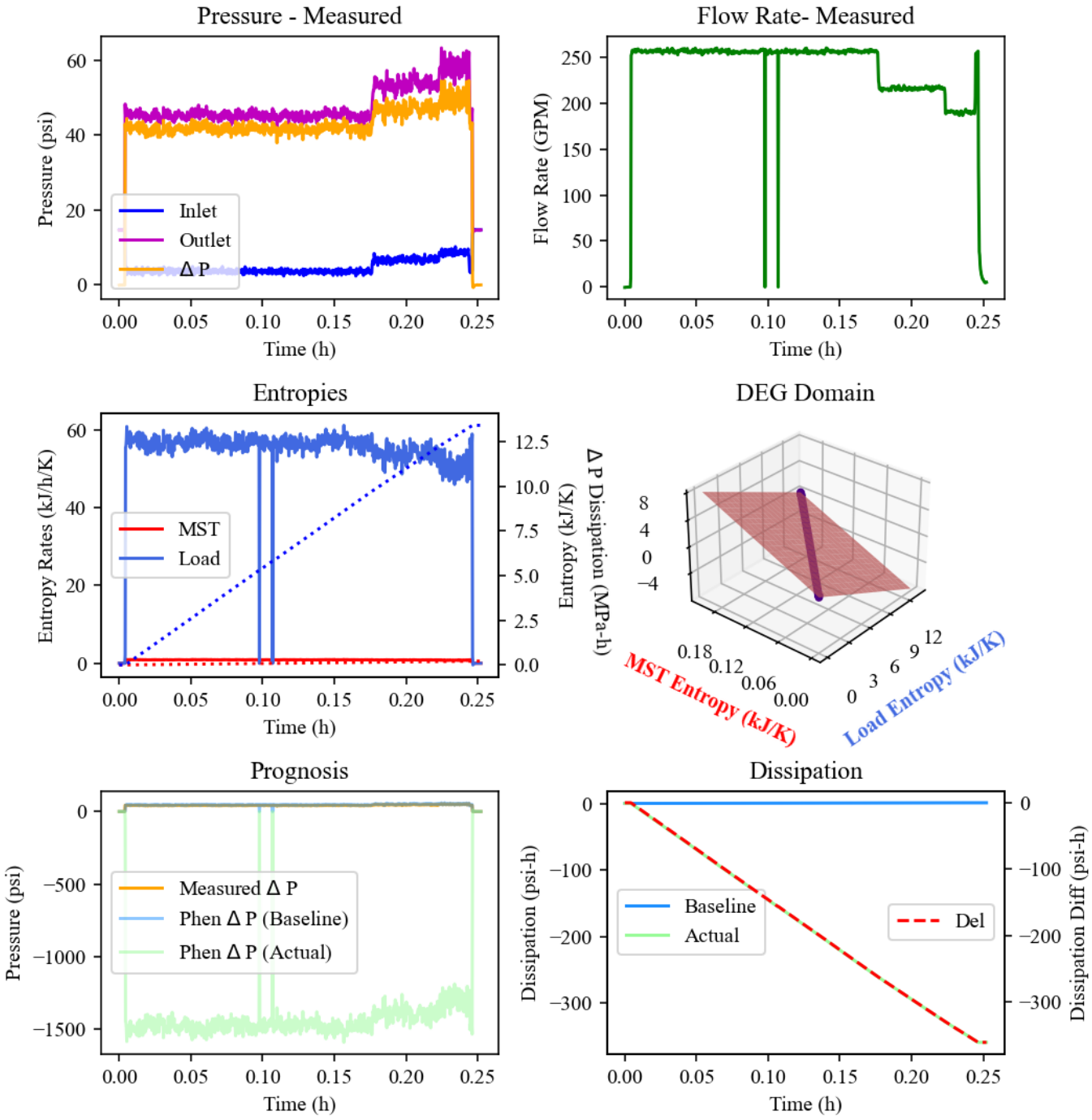

Copyright© 2021 by Turbomachinery Laboratory, Texas A&M Engineering Experiment Station

e) Phase Unbalance

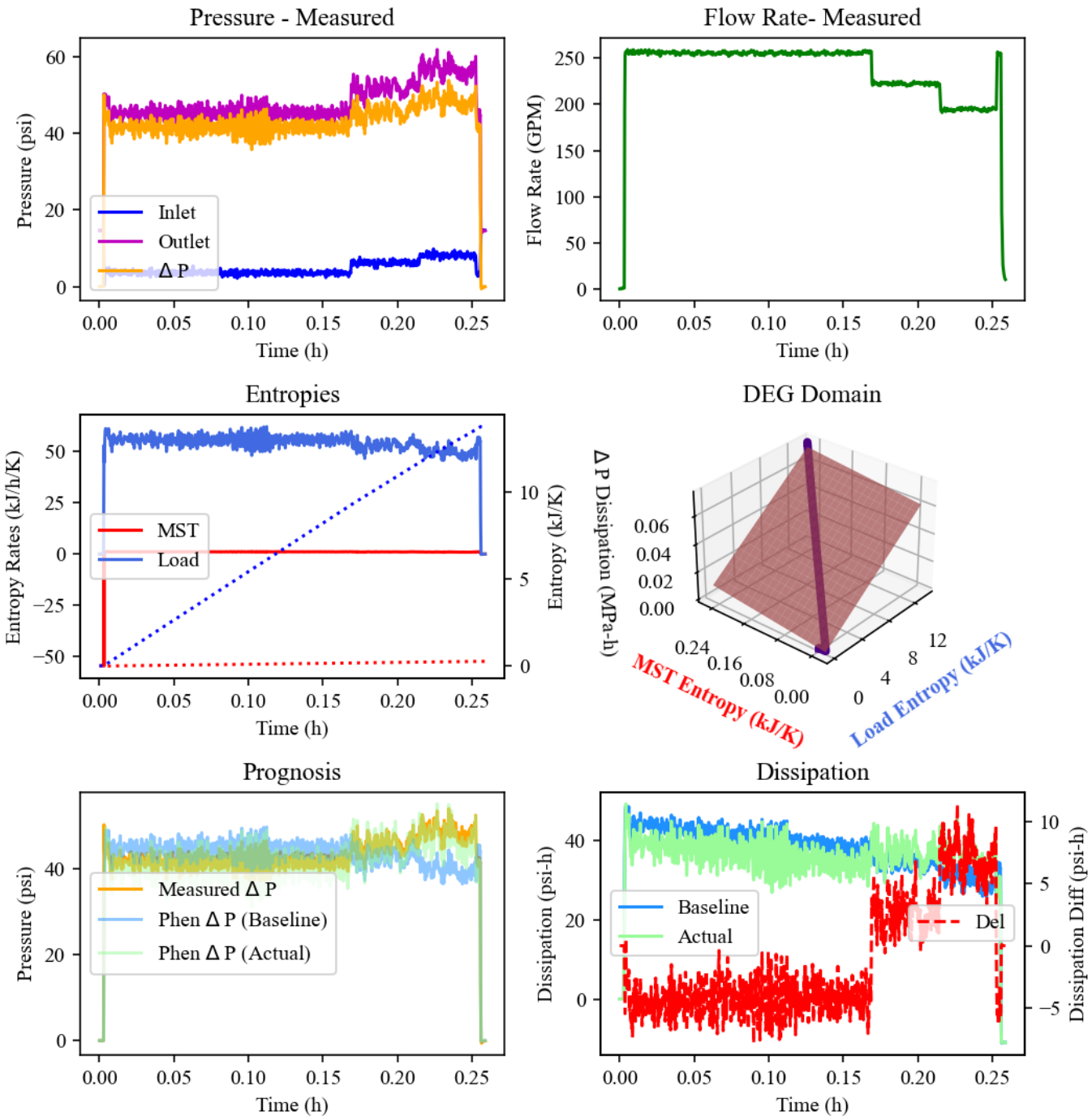

Figure 16. Typical components of a DEG Analysis. Monitored parameters include inlet and exit pressures, volumetric flow rate and ambient temperature. Shown are DEG elements (entropies, DEG domain, phenomenology and dissipation), for all the investigated conditions for (a) healthy, (b) soft foot, (c) misalignment, (d) shaft imbalance, *and (e) phase Unbalance*.

REFERENCES

Amiri M, Khonsari MM. Life prediction of metals undergoing fatigue load based on temperature evolution. Materials Science and Engineering A 2010;527:1555–9. doi:10.1016/j.msea.2009.10.025.

Amiri M, Modarres M. An entropy-based damage characterization. Entropy 2014;16:6434–63. doi:10.3390/e16126434.

Copyright© 2021 by Turbomachinery Laboratory, Texas A&M Engineering Experiment Station

Amiri M, Naderi M, Khonsari MM, Amiri M. NMKMM, M. A, M N, et al. An Experimental Approach to Evaluate the Critical Damage. International Journal of Damage Mechanics 2011;20:89–112. doi:10.1177/1056789509343082.

Basaran C, Lin M, Ye H. A thermodynamic model for electrical current induced damage 2003;40:7315–27. doi:10.1016/j.ijsolstr.2003.08.018.

Basaran C, Nie S. An Irreversible Thermodynamics Theory for Damage Mechanics of Solids. International Journal of Damage Mechanics 2004. doi:10.1177/1056789504041058.

Basaran C, Gomez J, Gunel E, Li S. Thermodynamic Theory for Damage Evolution in Solids. In: Voyiadjis G, editor. Handbook of Damage Mechanics, New York: Springer; 2014, p. 721–62. doi:10.1007/978-1-4614-8968-9.

Bryant Michael, Khonsari M. , and Ling F. On the thermodynamics of degradation. Proceedings of The Royal Society A: Mathematical, Physical and Engineering Sciences, 464:2001–2014, 08 2008.

Bryant Michael D. and Choi Ji Hoon . Model-based fault diagnostics of induction motor and centrifugal pump. In Prognostics and Health Management Solutions Conference, 12 2012. Prognostics and Health Management Solutions Conference - PHM: Driving Efficient Operations and Maintenance, MFPT 2012 ; Conference date: 24-04-2012 Through 26-04-2012.

Bryant Michael D. A data driven method for model based diagnostics and prognostics. In Annual Conference of the Prognostics and Health Management Society 2014. Prognostics and Health Management Society 2014, 2014.

Costuros Theodossios Vlasios . Application of Communication Theory to Health Assessment, Degradation Quantification, and Root Cause Diagno- sis. PhD thesis, The University of Texas at Austin, 2013.

Geiger G. Monitoring of an electrical driven pump using continuous-time parameter estimation methods. IFAC Proceedings Volumes, 15(4):603 – 608, 1982. 6th IFAC Symposium on Identification and System Parameter Estimation, Washington USA, 7-11 June.

Isermann R. and Freyermuth B.. Process Fault Diagnosis Based on Process Model Knowledge: Part IICase Study Experiments. Journal of Dynamic Systems, Measurement, and Control, 113(4):627–633, 12 1991.

Kuhn E. Tribological Stress of Lubricating Greases in the Light of System Entropy 2016:1–12. doi:10.3390/lubricants4040037.

Kuhn E. Correlation between System Entropy and Structural Changes in Lubricating Grease. Lubricants 2015; 3:332–45. doi:10.3390/lubricants3020332.

Kuhn E. Application of a Thermodynamic Concept for the Analysis of Structural Degradation of Soap Thickened Lubricating Greases 2018. doi:10.3390/lubricants6010007.

Morrow J. Cyclic Plastic Strain Energy and Fatigue of Metals. ASTM International 1965.

Naderi M, Khonsari MM. An experimental approach to low-cycle fatigue damage based on thermodynamic entropy. International Journal of Solids and Structures 2010;47:875–80. doi:10.1016/j.ijsolstr.2009.12.005.

Naderi M, Khonsari MM. A thermodynamic approach to fatigue damage accumulation under variable loading. Materials Science and Engineering A 2010;527:6133–9. doi:10.1016/j.msea.2010.05.018.

Naderi M, Amiri M, Khonsari MM. On the thermodynamic entropy of fatigue fracture. Proceedings of the Royal Society A: Mathematical, Physical and Engineering Sciences 2010;466:423–38. doi:10.1098/rspa.2009.0348.

Naderi M, Khonsari MM. Thermodynamic analysis of fatigue failure in a composite laminate. Mechanics of Materials 2012;46:113–22. doi:10.1016/j.mechmat.2011.12.003.

Naderi M, Khonsari M. Real-time fatigue life monitoring based on thermodynamic entropy. Structural Health Monitoring 2011;10:189–97. doi:10.1177/1475921710373295.

Naderi M, Khonsari MM. A comprehensive fatigue failure criterion based on thermodynamic approach. Journal of Composite Materials 2012;46:437–47. doi:10.1177/0021998311419540.

Naderi M, Khonsari MM. On the role of damage energy in the fatigue degradation characterization of a composite laminate. Composites Part B: Engineering 2013;45:528–37. doi:10.1016/j.compositesb.2012.07.028.

Osara Jude Asuelimen . The Thermodynamics Of Degradation. PhD thesis, The University of Texas at Austin, 2017.

Copyright© 2021 by Turbomachinery Laboratory, Texas A&M Engineering Experiment Station

Osara J.A., Bryant M.D., Thermodynamics of Lead-Acid Battery Degradation : Application of the Degradation-Entropy Generation Methodology, 166 (2019). doi:10.1149/2.0651916jes.

Osara J.A., Bryant M.D., A Thermodynamic Model for Lithium-Ion Battery Degradation : Application of the Degradation-Entropy Generation Theorem, Inventions. 2 (2019).

Osara J, Bryant M, Thermodynamics of Fatigue: Degradation-Entropy Generation Methodology for System and Process Characterization and Failure Analysis, Entropy. 21 (2019) 685. doi:10.3390/e21070685.

Osara J.A., Bryant M.D., Thermodynamics of grease degradation, Tribology International. 137 (2019) 433–445. doi:10.1016/j.triboint.2019.05.020.

Osara J.A., Bryant M.D, Performance and degradation characterization of electrochemical power sources, Electrochemica Acta. 137 (2020).

Osara J.A., Bryant M.D. Degradation Thermodynamics: Systems and Methods for Degradation Analysis. In submission. 2021

Rezasoltani A, Khonsari MM. An engineering model to estimate consistency reduction of lubricating grease subjected to mechanical degradation under shear. Tribology International 2016;103:465–74. doi:10.1016/j.triboint.2016.07.012.

Rincon Juan Sebastian . Comprehensive Framework for Machine Diagnosis & Prognosis. Master's Thesis, The University of Texas at Austin, 2020.

Shannon Claude E. . A Mathematical Theory of Communication, volume 27. The Bell System Technical Journal, 1948.

Shannon Claude E. . Communication in the presence of noise. Proceedings of the IEEE, 86(2): 447–457, 1998. (A reprint from the *PROCEEDINGS OF THE IRE*, vol. 37, no. 1, pp. 10–21, Jan. 1949.)

SKF Reliability Systems. Vibration Diagnostic Guide. 2000.

Thomsen J. S. and Kallesoe C. S. Stator fault modeling in induction motors. In International Symposium on Power Electronics, Electrical Drives, Automation and Motion, 2006. SPEEDAM 2006., pages 1275– 1280, 2006.

ACKNOWLEDGEMENTS

The team would like to thank Mechanical Solutions Inc. for their support and assistance in testing these methodologies.

Copyright© 2021 by Turbomachinery Laboratory, Texas A&M Engineering Experiment Station